Gaps and kinks in the electronic structure of the superconductor 2H-NbSe_{2} from angle-resolved photoemission at 1 K

D. J. Rahn, S. Hellmann, M. Kalläne, C. Sohrt, T. K. Kim, L. Kipp, and K. Rossnagel

Phys. Rev. B **85**, 224532 — Published 26 June 2012

DOI: 10.1103/PhysRevB.85.224532

Gap and kink structure of the layered superconductor $2H$-NbSe$_2$ from angle-resolved photoemission at 1 kelvin

D. J. Rahn,[1] S. Hellmann,[1] M. Kalläne,[1] C. Sohrt,[1] T. K. Kim,[2,*] L. Kipp,[1] and K. Rossnagel[1,†]

[1] *Institute of Experimental and Applied Physics, University of Kiel, 24098 Kiel, Germany*
[2] *Leibniz Institute for Solid State and Materials Research Dresden, 01171 Dresden, Germany*

Angle-resolved photoemission spectroscopy at a temperature of 1 K is used to determine the wavevector dependence of the spectral gap and band renormalization due to electron-phonon coupling in the layered charge-density-wave superconductor $2H$-NbSe$_2$. The measured gap size and coupling parameter are Fermi-surface-sheet dependent and anisotropic. The largest energy gap, highest coupling strength, and strongest variation in both quantities are found on the double-walled Nb $4d$-derived Fermi-surface sheet that is centered on the corners of the hexagonal Brillouin zone. On this sheet, the spectral gap has two distinct anticorrelated components associated with superconductivity and the charge-density wave. The results establish $2H$-NbSe$_2$ as a moderately correlated intermediate-coupling anisotropic multi-gap superconductor.

PACS numbers: 74.70.Ad,74.25.Jb,71.45.Lr,79.60.–i

I. INTRODUCTION

$2H$-NbSe$_2$ is a layered, conventional, low-temperature superconductor ($T_c = 7.3$ K)[1] with a multi-sheet Fermi surface consisting of a Se $4p$ "pancake" and two double-walled Nb $4d$ cylinders[2–4] and with an incommensurate charge-density-wave (CDW) phase ($T_0 = 33.5$ K)[5] coexisting with superconductivity. Because of the latter two characteristics, the material is often said to share similarities with fashionable high-temperature superconductors such as MgB$_2$, the copper oxides, or the iron pnictides/chalcogenides. However, before $2H$-NbSe$_2$ qualifies as a reference system, some central questions related to its superconducting (SC) ground state should be answered conclusively, namely: (i) What is the structure, magnitude, and degree of anisotropy of the energy gap in wavevector (**k**) space? (ii) Does the CDW impede or assist superconductivity? And (iii) how is the gap structure related to the nesting properties of the Fermi surface and the **k**-dependent "kinking" of the band dispersions due to electron-phonon coupling? In addition to generally allowing for a better identification of truly unconventional effects in high-temperature superconductors, the answers to (i)–(iii) would specifically help to understand why the T_c of $2H$-NbSe$_2$ is the highest within the family of transition-metal dichalcogenides.[1]

At first glance it seems surprising that the above questions are still largely open although many different sorts of experiments have been performed on $2H$-NbSe$_2$, including specific heat,[6] thermal conductivity,[7] magnetization,[8] and penetration depth[9] measurements, as well as tunneling spectroscopy[10–13] and angle-resolved photoemission spectroscopy (ARPES).[14–17] But much of the discord can indeed be traced back either to the lack of **k** resolution of the experimental probes or to the relatively high temperatures ($\gtrsim 0.7\,T_c$) at which the ARPES measurements[14–17] were done.

To resolve the situation, we have performed ARPES on $2H$-NbSe$_2$ at a temperature of 1 K ($=0.14\,T_c$) and comprehensively determined the **k**-dependent fine structure of the low-energy electronic structure. The SC gap is shown to have multiple Nb $4d$-derived components and a strong anisotropy—including gapless regions—that appears to be correlated with the **k** dependence of the band modification by phonon kinks. The SC gap is also seen to have a highly **k**-selective competitor: the CDW gap. Yet, the rather surprising reason for the comparatively high T_c of $2H$-NbSe$_2$ turns out to be that the CDW, as the supposedly stronger competitor, is also a supporter of superconductivity, as it leaves most of the Fermi surface intact.

Our paper is structured as follows. After a detailed description of the methods in Sec. II, we will briefly reexamine the undistorted electronic structure of $2H$-NbSe$_2$ near the Fermi energy (E_F) in Sec. III A. We will then present the effects of electron-phonon coupling deep in the SC phase at a temperature of 1 K: the band renormalization on approaching E_F in Sec. III B and, our most important experimental result, the structure of the energy gap at E_F in Sec. III C.

II. METHODS

The single-crystal samples used in the experiments reported here were grown via iodine vapor transport and had a T_c of 7.3 K confirmed by transport measurements. Low-temperature (1 K) and intermediate-temperature (3.5–55 K) ARPES was performed at beamline UE112-PGM-2b of BESSY II (Berlin) at photon energies of $h\nu = 23$ and 55 eV with total energy resolutions of $\Delta E = 3.8$ and 8 meV, respectively. The smallest measured momentum-distribution-curve was $\Delta k_{\|} = 0.04$ Å^{-1}. High-temperature (60 K) measurements were done at beamline 7.0.1 of the Advanced Light Source (Berkeley) at $h\nu = 132$ eV, $\Delta E = 50$ meV, and $\Delta k_{\|} = 0.07$ Å^{-1}. Both experiments feature a Scienta R4000 spectrometer, and the one in Berlin a Janis ^{3}He cryostat.

Our quantitative analysis of the measured ARPES data employs standard procedures and focuses on the $\mathbf{k}$ dependence of five key quantities of a CDW superconductor: the undistorted band structure near E_F, the electron-phonon coupling parameter, the spectral gap, the SC coherent spectral weight, and the bare susceptibility at the wavevector of the CDW.

To reproduce the band dispersion and Fermi surface of the two lowest-lying Nb $4d$-derived states of $2H$-NbSe$_2$, we use a two-dimensional fifth-nearest-neighbor tight-binding model based on the fitting scheme originally proposed in Ref. 18 and later successfully employed in Refs. 19–21:

$$\begin{aligned} E(\mathbf{k}) = t_0 &+ t_1\,(2\cos\xi\cos\eta + \cos 2\xi) \\ &+ t_2\,(2\cos 3\xi\cos\eta + \cos 2\eta) \\ &+ t_3\,(2\cos 2\xi\cos 2\eta + \cos 4\xi) \\ &+ t_4\,(\cos\xi\cos 3\eta + \cos 5\xi\cos\eta + \cos 4\xi\cos 2\eta) \\ &+ t_5\,(2\cos 3\xi\cos 3\eta + \cos 6\xi) \end{aligned} \tag{1}$$

where $\mathbf{k} = (k_x, k_y)$ denotes the wavevector parallel to the hexagonal Nb layers, $\xi = \frac{1}{2}k_x a$, and $\eta = \frac{1}{2}\sqrt{3}k_y a$ (a: lattice parameter). Note that the corresponding formula given in Ref. 21 contains the t_4 and t_5 terms in different order and a typo in the t_4 term. In our fitting scheme, all coefficients t_i are treated as fit parameters. Their optimum values for the two Nb bands are determined by fitting the model function (1) to the positions of the respective local intensity maxima in the complete high-temperature ARPES data set, while restricting the band energies at the high-symmetry points in the unoccupied region to values calculated within the local-density approximation (LDA).[24]

To determine the variation of the electron-phonon coupling parameter λ along the Fermi contours (of the low-temperature ARPES data set), we assume that the band renormalization near E_F is for the most part due to electron-phonon coupling so that the strength of the renormalization of the Fermi velocity becomes a direct measure of λ:

$$\lambda = \frac{v_F^0}{v_F^*} - 1, \tag{2}$$

where v_F^0 and v_F^* are the bare and renormalized Fermi velocity, respectively.[15,16] Since the bands crossing E_F in $2H$-NbSe$_2$ are steep, we can extract the renormalized ("kinked") band dispersions from appropriate E-versus-k ARPES intensity maps by momentum-distribution-curve fitting, i.e., by fitting Lorentzians (plus a linear background) to each constant-E profile of the maps. The parameters v_F^0 and v_F^* are then determined by fitting lines, which are forced through the Fermi-level crossing, to different portions of the extracted band dispersion: v_F^0 is evaluated from an energy interval well below E_F, typically ranging from -100 to -90 meV, and v_F^* from the energy window spanned by the highest kink energy and E_F. The absolute error in the determination of λ is estimated to be ±0.1.

To determine the relative and absolute variation of the spectral gap Δ on the Fermi surface, we use two common gap indicators: the position of the inflection point of the leading edge as obtained from simple Fermi-edge fitting and the gap value determined by more elaborate lineshape analysis employing the phenomenological self-energy model introduced in Ref. 22:

$$\Sigma(\mathbf{k},\omega) = -i\Gamma_1 + \frac{\Delta^2}{\omega + E(\mathbf{k}) + i\Gamma_0}, \tag{3}$$

where ω measures energy relative to E_F and Γ_0 and Γ_1 are scattering rates commonly treated as fit parameters.[14,16] For the latter approach to be valid, we have to make two approximations: the general approximation that the measured ARPES intensity $I(\mathbf{k},\omega)$ is proportional to $A(\mathbf{k},\omega)f(\omega)$, where $A(\mathbf{k},\omega) = \frac{1}{\pi}\mathrm{Im}\,[\omega - E(\mathbf{k}) - \Sigma(\mathbf{k},\omega)]^{-1}$ is the spectral function, and the specific approximation that A is particle-hole symmetric for small $|\omega|$, i.e., $A(E(\mathbf{k}),\omega) = A(-E(\mathbf{k}),-\omega)$. The symmetrized ARPES intensity $I(\mathbf{k}_F,\omega) + I(\mathbf{k}_F,-\omega)$ at the Fermi vector $\mathbf{k}_F$ is then simply $A(\mathbf{k}_F,\omega)$ convolved with the resolution function of the experiment. In our fitting scheme, the parameter Γ_0 is set to zero and the energy interval of the fit is typically restricted to the width of

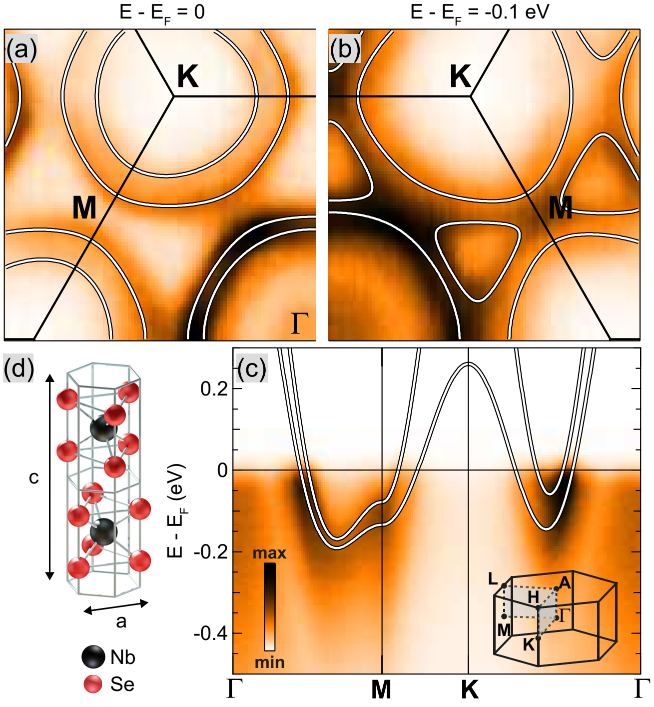

FIG. 1. (Color online). Measured ARPES intensity distributions of $2H$-NbSe$_2$ ($h\nu = 132$ eV, $T = 60$ K) versus fitted Nb $4d$ tight-binding band dispersions (white lines): (a), (b) select constant-energy contours and (c) band dispersion along the Γ-M-K-Γ high-symmetry path. The experimental data shown are averaged over symmetry-equivalent cuts of the full data set. (d) Real-space unit cell of $2H$-NbSe$_2$. Inset in (c): conventional three-dimensional Brillouin zone.

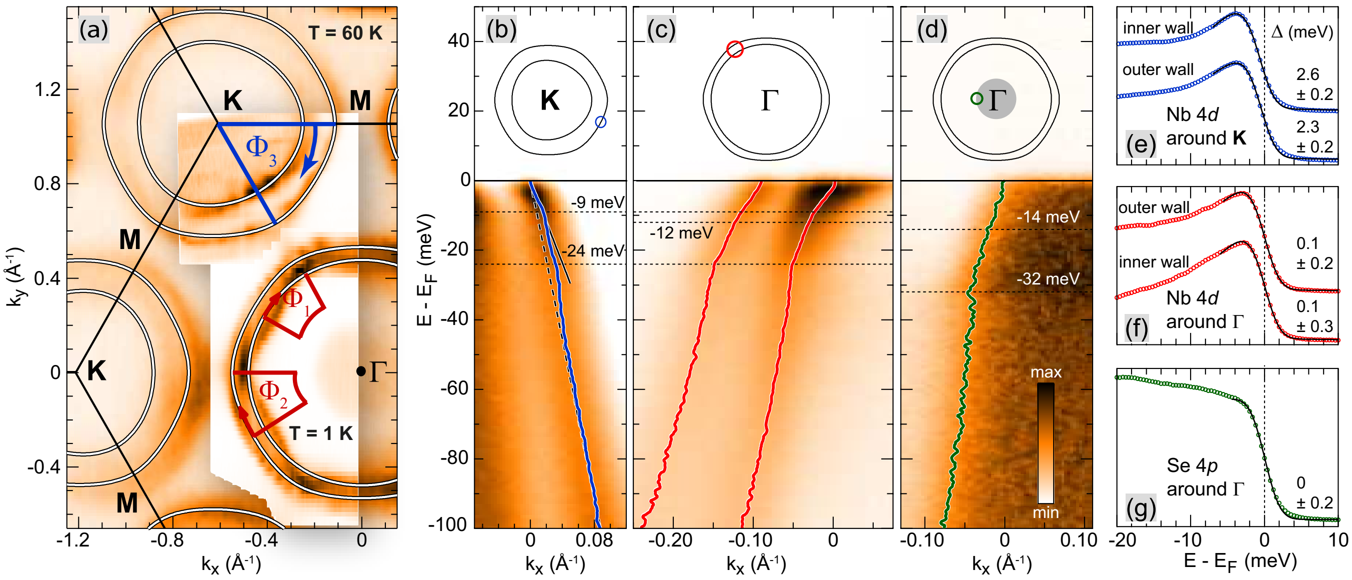

FIG. 2. (Color online). Fermi-surface-sheet dependence of the low-energy electronic structure of $2H$-NbSe$_2$ as seen by ARPES. (a) Fermi-surface maps measured at temperatures of 60 K (overview map; $h\nu = 132$ eV) and 1 K (highlighted area; $h\nu = 23$ eV). Best-fit tight-binding Fermi contours are overplotted. Arrows and angles Φ_i indicate Fermi-surface segments used for quantitative data analysis. (b)–(d) Three representative band maps ($h\nu = 23$ eV, $T = 1$ K) displaying Fermi-level crossings at the indicated Fermi vectors. Thick solid curves depict the band dispersions determined by momentum-distribution-curve fitting. Dashed horizontal lines mark kink energies. Long-dashed and solid straight lines in (a) indicate bare and renormalized Fermi velocities, respectively. (f)–(h) Fermi-surface-sheet averaged spectra ($h\nu = 23$ eV, $T = 1$ K). Energy-gap values (Δ) and estimated error bars obtained from lineshape analysis (best fits overplotted as thin solid lines) are indicated.

the SC coherent peak. The accuracy of the fitted Δ values is estimated to be ±0.2 meV. Note that Δ refers to the distance between the lower gap edge and E_F so that the total gap size is 2Δ. Also note that tunneling spectroscopy indicates a **k**-averaged CDW gap which is asymmetric and has its minimum located slightly above E_F.[10,11] For wavevectors at which the CDW contributes significantly to the opening of the spectral gap, the stated Δ values may therefore underestimate the total gap size.

To quantify the relative variation of the SC component of the spectral gap on the relevant Fermi-surface sheets, we rely on the spectral weight of the SC coherent peak which typically emerges as a resolution-limited feature on top of the conventional quasiparticle peak for temperatures below T_c.[23] In the absence of realistic self-energy models for coexisting SC and CDW ground states, this simple criterion appears to be the most effective and transparent one, although it may be hampered by background and matrix-element effects. To keep both effects to a minimum, we consider only a small energy window ($E_F \pm 40$ meV), normalize the symmetrized spectra to the intensity of the background, and determine only relative changes of the integrated spectral weight along segments of the Fermi contours on which the matrix element shows a weak **k** dependence (see Fig. 2(a) for the selection of Fermi-surface segments).

Finally, to identify potential CDW "hot spots" in the Nb 4d electronic structure near E_F, we decompose the bare susceptibility at the observed CDW wavevector, $\chi_0(\mathbf{q}_0)$, into **k**-dependent terms $\Omega(\mathbf{k})$ which we calculate from the fitted tight-binding band energies:

$$\chi_0(\mathbf{q}_0) = \sum_{\mathbf{k}} \Omega(\mathbf{k}),$$
$$\Omega(\mathbf{k}) = \sum_{\lambda,\lambda',i} \frac{f(\mathbf{k}+\mathbf{q}_i\lambda') - f(\mathbf{k}\lambda)}{E(\mathbf{k}\lambda) - E(\mathbf{k}+\mathbf{q}_i\lambda')}, \tag{4}$$

where f denotes the Fermi-Dirac function and the indices $\lambda, \lambda' = 1, 2$ and $i = 0, 1, 2$ run over the two Nb 4d bands and the three wavevectors of the incommensurate triple-**q** CDW, respectively ($\mathbf{q}_1$ and $\mathbf{q}_2$ have the same magnitude as $\mathbf{q}_0 = \frac{4\pi}{\sqrt{3}a}(0.327, 0, 0)$, but are rotated by ±120° about the k_z-axis[5]). In a simple nesting scenario, large values of $\Omega(\mathbf{k})$ would indicate well-nested sections of the Fermi surface on which the CDW gap is expected to open up.

III. RESULTS AND DISCUSSION

A. Fermi surface and band structure

The double trilayer structure of $2H$-NbSe$_2$ with its two Nb atoms per unit cell [Fig. 1(d)] corresponds with a predominantly quasi-two-dimensional Fermi surface that is dominated by double-walled Nb 4d-derived cylinders centered on the Γ–A and K–H lines of the Brillouin zone.[2–4] In ARPES Fermi-surface cuts, such as

TABLE I. Best-fit tight-binding parameters for the two lowest-lying Nb $4d$-derived bands of $2H$-NbSe$_2$. All parameters in meV, for a lattice parameter of $a = 3.444$ Å.

	t_0	t_1	t_2	t_3	t_4	t_5
band 1	10.9	86.8	139.9	29.6	3.5	3.3
band 2	203.0	46.0	257.5	4.4	−15.0	6.0

the ones shown in Figs. 1(a) and 2(a), these Nb sheets are typically well resolved, whereas a further, smaller, three-dimensional sheet around the Γ point—the Se $4p_z$-derived “pancake”—generally appears blurred due to k_z broadening.[3,14–17,19,20,25–27] Since for $2H$-NbSe$_2$ the k_z dispersion of the Nb $4d$ states is weak[3] and the effective k_z resolution is in the order of the k_z extension of the Brillouin zone, the Nb $4d$ contours in the Fermi-surface maps may, to a good approximation, be interpreted as k_z averages.

We obtain the best tight-binding simulation of the two Nb $4d$ bands in the vicinity of E_F for the parameters listed in Tab I. Corresponding band dispersions and constant-energy contours are included in Figs. 1(a)–1(c) and confirm that the tight-binding model (1) can comprehensively capture the occupied part of the Nb $4d$ band structure as seen by ARPES above T_0.[19,20] The Nb $4d$ band minimum is found at about $\frac{2}{3}$ along the Γ-M line and the occupied Nb $4d$ band width is $W_{ARPES} = 0.19$ eV. What seems to not have been appreciated before, is that the ratio of the k_z-averaged Nb $4d$ band widths measured by ARPES and calculated within LDA[2–4] is significantly smaller than one: $W_{ARPES}/W_{LDA} = 0.45 \pm 0.12$. This places $2H$-NbSe$_2$ in the moderately correlated regime.[28]

Figure 2(a) shows that upon cooling to the lowest temperature currently achievable in ARPES experiments ($T = 1$ K), the shape and size of the maximum intensity contours in the Fermi-surface map are largely preserved. Yet, intriguingly, all bands sharpen up significantly [Figs. 2(b)–2(d)] and a distinct electronic fine structure appears comprising Fermi-surface-sheet dependent kink and gap sub-structures [Figs. 2(b)–2(g)].

B. Kink structure

Figures 2(b)–2(d) illustrate the momentum-distribution-curve analysis of the electronic structure in an 100 meV wide energy window below E_F for characteristic slices of the low-temperature data set. The fitted peak positions quantify the measured band dispersions and reveal significant renormalization of the Fermi velocities due to the emergence of distinct multiple kinks.

The full **k** dependence of the band renormalization is displayed in Figs. 3(d)–3(f), except for the inner K-H-centered Nb Fermi-surface sheet for which we were not able to determine accurate band dispersions. For each group of Fermi contours, the kinks occur at characteristic energies: for the Se Γ pocket at 14 and 32 meV and for the double-walled Nb Γ-A and K-H pockets at 9, 12, and 24 meV and at 9 and 24 meV, respectively. This range of kink energies agrees with previous results obtained from less sharp Nb bands with single kinks only.[15] All kink positions are consistent with the energies of optic and acoustic phonon modes at the corresponding wavevectors.[29,30]

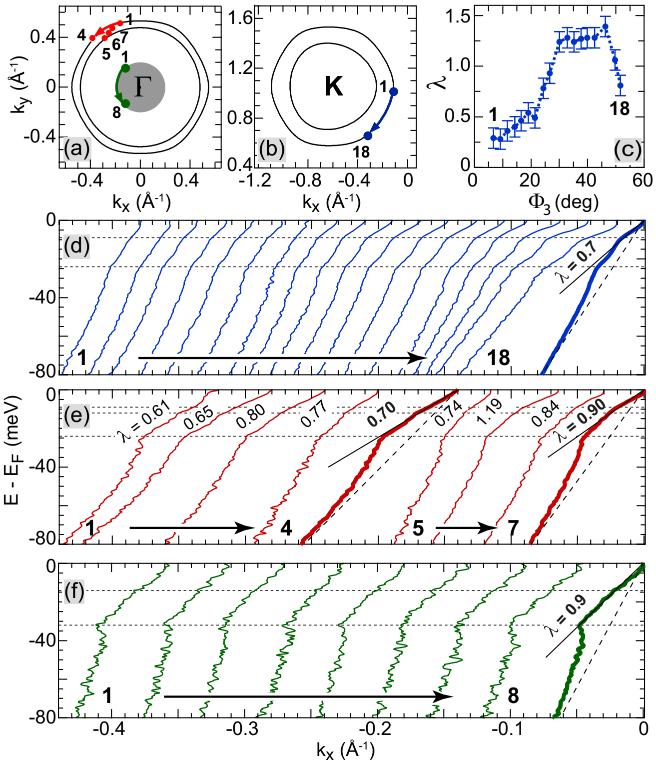

FIG. 3. (Color online). Wavevector dependence of the mass enhancement parameter (λ) on the three groups of Se $4p$- and Nb $4d$-derived Fermi-surface sheets ($h\nu = 23$ eV, $T = 1$ K). (a), (b) Locations of the analyzed Fermi-level crossings. (c) Variation of λ on the outer K-H-centered Nb $4d$ Fermi contour. (d)–(f) Extracted band dispersions as a function of position on the Fermi surface. Thick solid lines represent Fermi-surface-sheet-averaged dispersions. Short-dashed horizontal lines mark the energy positions of kinks. Mass enhancement parameter values as determined from Fermi velocity changes (long-dashed and solid straight lines) are indicated.

Figure 3 and Tab. II lay out the **k** dependence of the electron-phonon coupling parameter λ, determined from Fermi-velocity changes. As pointed out before,[15] it is interesting to note that despite the anticipated anisotropy of the electron-phonon interaction and the observed Fermi-surface-sheet dependence of the kink energies, λ varies only little along some sheets and between different sheets. In agreement with previous, less systematic ARPES studies,[15,16] the Fermi-surface-sheet averages of λ are in the range of 0.7–0.9 and the variations along individual contours are limited to ±33%, except

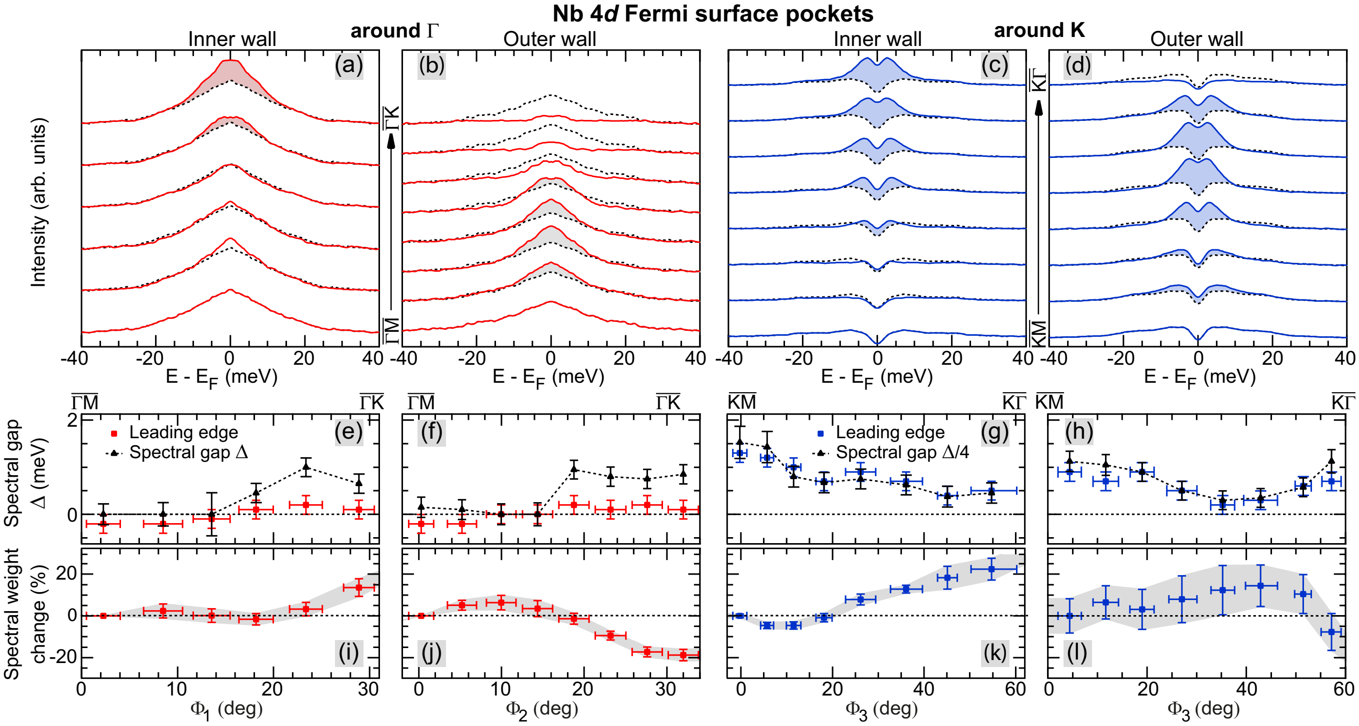

FIG. 4. (Color online). Wavevector dependence of the spectral gap on the four Nb $4d$-derived Fermi-surface sheets ($h\nu = 23$ eV, $T = 1$ K). (a)–(d) Symmetrized energy-distribution curves measured along the paths indicated in Fig. 2(a). Dashed-line spectra are replica of the spectrum at the bottom of each panel. Filled areas highlight spectral weight changes (light gray filling in (b) indicates anomalous changes, see text). (e)–(h) Leading-edge positions and spectral-gap values extracted from the curves in (a)–(d). Note that in (g) and (h) $\Delta/4$ is plotted. (i)–(l) Energy-integrated spectral weight changes relative to the bottom spectra in (a)–(d) (interval of integration: -40 to $+40$ meV). Estimated error bars are shown in (e)–(l).

for the outer K-H Nb pocket where deviations from the average value of up to +100% are detected [Fig. 3(c)]. Remarkably, in trying to correlate the measured coupling parameter with the experimental T_c, we find that the local maxima of the spectroscopic λ are consistent with the empirical $\lambda = 1.3 \pm 0.1$ calculated from McMillan's formula (using a Debye energy of 19 meV (Ref. 6) and assuming a Coulomb repulsion parameter μ^* in the range of 0.1–0.2.).[31]

C. Gap structure

Compared to the electron-phonon coupling strength, the measured spectral gap shows a much stronger Fermi-surface-sheet dependence. The sheet-averaged gap size increases monotonously towards the edges of the Brillouin zone, growing from zero on the Se Γ pocket[14,16] to a small value (∼0.1 meV) on the Nb Γ-A sheets and reaching 2.6 meV on the Nb K-H contours [Figs. 2(e)–2(g) and Tab. II]. Such a "two-gap scenario" is qualitatively consistent with what **k**-integrated experimental probes tend to measure.[6–9,12,13]

Intriguingly, the Fermi-surface-sheet selectivity of the gap comes along with a significant variation of the gap along the various Nb pockets.[12,16,17] The qualitative behavior is illustrated in Figs. 4(a)–4(d) for all four Nb sheets by plotting symmetrized spectra measured around each contour. The quantitative analysis is presented in Figs. 4(e)–4(l) which compare the Fermi-angle dependence of the position of the inflection point of the leading edge, the gap value determined by self-energy fitting, and the spectral weight of the SC coherent peak emerging at the gap edge.[14,16,17,23] As to the reliability of the data analysis scheme detailed in Sec. II, three aspects are worth noting: (i) There is an almost perfect correlation between the fitted gap values and leading-edge shifts on all four Fermi-surface sheets [Figs. 4(e)–4(h)]. (ii) The spectral weight changes are indeed restricted to a narrow energy window around E_F corresponding to the width of the SC coherent peak [Figs. 4(a)–4(d)]. (iii) Any anomaly

TABLE II. Fermi-surface-sheet dependence of the measured spectral gap Δ and mass enhancement parameter λ. Average values plus maximum and minimum deviations are given.

	Se 4p	Nb 4d around Γ		Nb 4d around K	
		inner	outer	outer	inner
Δ (meV)	0	$0.1^{+0.9}_{-0.1}$	$0.1^{+0.9}_{-0.1}$	$2.3^{+2.2}_{-1.1}$	$2.6^{+3.5}_{-1.1}$
λ	0.9	$0.9^{+0.3}_{-0.2}$	$0.7^{+0.1}_{-0.1}$	$0.7^{+0.7}_{-0.4}$	—

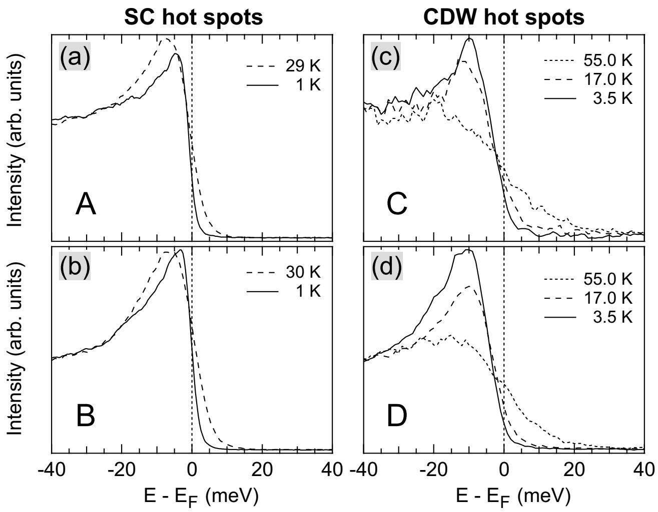

FIG. 5. Temperature-dependent ARPES spectra at selected positions on the Nb $4d$-derived Fermi surface (marked as points A–D in Fig. 6): (a), (b) superconducting (SC) hot spots ($h\nu = 23$ eV, $\Delta E = 3.8$ meV) and (c), (d) charge-density-wave (CDW) hot spots ($h\nu = 55$ eV, $\Delta E = 8$ meV).

due to background or matrix-element effects may affect the integrated spectral intensities, as, e.g., on the outer Γ-A Nb contour near the Γ-K line [Figs. 4(b) and 4(j)], but not the fitted leading-edge positions and spectral-gap values [Fig. 4(f)].

The quantitative analysis reveals the complex structure of the spectral gap with its anisotropy and Fermi-surface-sheet dependence in full detail. On both Γ-A contours, the spectral gap is zero within the error bars near the Γ-M line and increases towards the Γ-K line [Figs. 4(e) and 4(f)]. Since the coherent spectral weight shows a similar behavior on the inner contour [Fig. 4(i)] and since the maximum gap values agree well with the expected mean-field SC gap ($1.76\,k_BT_c = 1.1$ meV), we tentatively attribute the observed gapping entirely to superconductivity.

The situation on the K-H sheets is remarkably different in three respects.[32] First, the spectral gap does not go to zero [Figs. 4(g) and 4(h)]. Second, the spectral gap and the coherent spectral weight are strongly anticorrelated [Figs. 4(g), 4(h), 4(k), and 4(l)]. And third, the maximum gap values are now more consistent with the expected mean-field CDW gap ($1.76\,k_BT_0 = 5.1$ meV). We are thus led to conclude that the spectral gap on the K-H sheets has two competing components: a SC gap and a CDW gap. The hot spots of the CDW gap are around the K-M line (both sheets) and K-Γ line (outer sheet), where the spectral gap is largest and the SC coherent peak is strongly suppressed.[17] Although a clean spectral decomposition is not possible, we tentatively assign a maximum value of 2.5 meV to the SC gap on the K-H sheets ($2\Delta_{SC,max}/k_BT_c \approx 8$), which would indicate intermediate-coupling superconductivity.

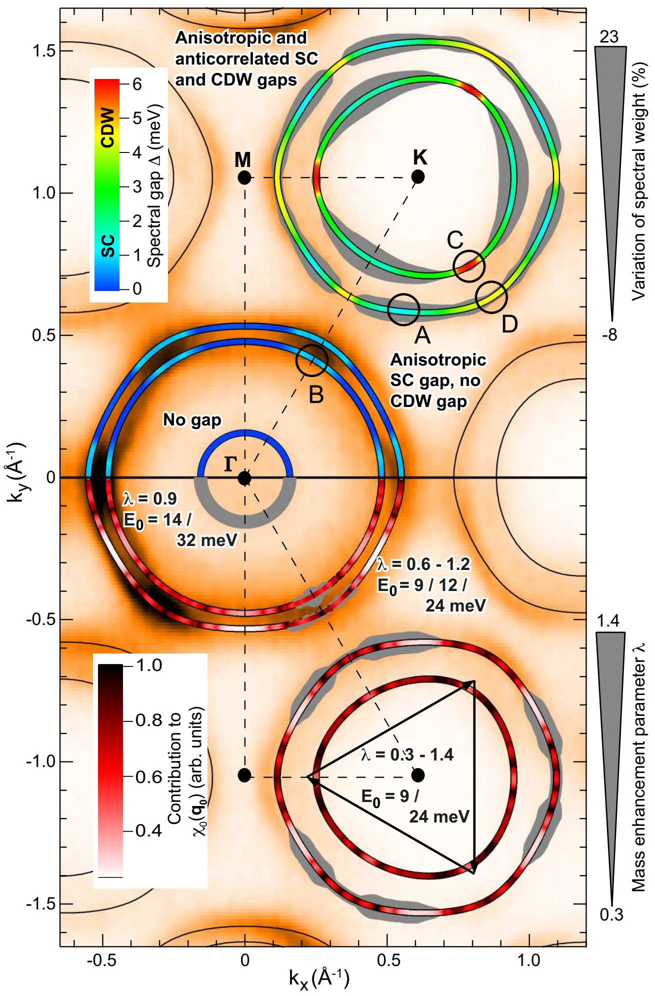

FIG. 6. Summary of the obtained ARPES results on $2H$-NbSe$_2$: wavevector dependences of the spectral gap (Δ) and superconducting (SC) coherent spectral weight (upper panel) and of the mass enhancement parameter (λ) and the contributions building up the bare susceptibility at the wavevector of the charge-density wave (CDW) [$\chi_0(\mathbf{q}_0)$] (lower panel). The kink energies (E_0) on the different Fermi-surface sheets and a group of wavevectors characterizing the triple-$\mathbf{q}$ CDW are also indicated. Circles labeled A–D mark the SC and CDW hot spots at which the temperature-dependent spectra in Fig. 5 were taken.

The qualitative decomposition into SC and CDW components suggested by the spectral weight analysis at fixed temperature is corroborated by Figs. 5(a)–5(d) showing ARPES spectra which were taken for select temperatures at characteristic points on the Nb $4d$ Fermi surface, labeled as A–D in Fig. 6. At points A (outer K-H pocket) and B (inner Γ-A pocket) at which the SC gap component should predominate, the gap is indeed closed at temperatures $T_c < T < T_0$, as indicated by the shift of the inflection point of the leading edge and by the broadening of the narrow SC coherent peak into a conventional quasiparticle peak [Figs. 5(a) and 5(b)]. By clear contrast, at the CDW hot spots C (inner K-H pocket) and D (outer K-H pocket), the leading-edge gap remains partially open in the temperature interval $T_c < T < T_0$ and has closed for a temperature higher than T_0 [Figs. 5(c) and 5(d)]. We note that the observed temperature dependence at the selected points is qualitatively consistent with previously published results.[14,16,17]

In Fig. 6, we visualize the key quantities measured in this work as a function of position on the Fermi surface: the electron-phonon coupling parameter λ, the spectral gap Δ, and the integrated coherent spectral weight. We also display where significant ("well-nested") contributions $\Omega(\mathbf{k})$ to the bare susceptibility at the observed CDW wavevector $\chi_0(\mathbf{q}_0)$ arise.[33] Intuitively, one would expect that at any given $\mathbf{k}$ a high λ would bring about a large SC component of Δ, while a large $\Omega(\mathbf{k})$ would translate into a large CDW component of Δ. But this is only partially so. Comparing the $\mathbf{k}_{\|}$ dependences of the depicted quantities, we find a distinct correlation between the SC gap (coherent spectral weight) and λ on the outer K-H Nb sheet, but no clear correlation between the CDW gap (largest gap sizes) and $\Omega(\mathbf{k})$. The largest contributions to $\chi_0(\mathbf{q}_0)$ do not originate exactly from the CDW hot spots and there are sections on the Fermi surface (particularly on the Γ-A Nb sheets) that contribute significantly to $\chi_0(\mathbf{q}_0)$ but are not gapped by the CDW. These observations are inconsistent with Fermi-surface nesting and point to an important role of the electron-phonon matrix element in determining the structure of the CDW gap and the observed $\mathbf{q}_0$.[34,35]

IV. CONCLUSIONS

In summary, our ultralow-temperature ARPES results show that the energy gap of $2H$-NbSe$_2$ has two anti-correlated principal components associated with superconductivity and the CDW. The smaller SC gap opens on all four Nb Fermi-surface sheets, but not on the Se pocket; it is generally anisotropic and includes gapless regions. The larger CDW gap, by contrast, opens only on a few hot spots on the Nb K-H sheets, suppresses the SC gap there, but otherwise leaves most of the Fermi surface to superconductivity. This dichotomy—competition and cooperation at the same time—explains the comparatively high T_c of $2H$-NbSe$_2$ within the family of transition-metal dichalcogenides in which commonly entire Fermi-surface pockets are gapped by the CDW.[36] However, while the anisotropy of the SC gap is partly reflected in the measured $\mathbf{k}$ dependence of the electron-phonon coupling parameter, there is no clear connection between the CDW gap and the nesting properties of the Fermi surface. In any forthcoming microscopic theory of the interplay between the CDW and superconductivity in $2H$-NbSe$_2$, it may become important to factor in that the material is in the moderately interacting regime regarding the overall strength of both electron-phonon and electron-electron interaction. We believe that our results on the intricate conventional superconductor $2H$-NbSe$_2$ provide a useful reference for the appraisal of electronic structure effects in unconventional superconductors. Regarding the technical innovation exploited in our work, we foresee that ARPES at 1 K will make a difference in the study of the electronic fine structure of superconductors and many other types of materials.

ACKNOWLEDGMENTS

This work was supported by the German BMBF (Project No. 05K10FK1). The Advanced Light Source is supported by the Director, Office of Science, Office of Basic Energy Sciences, of the U.S. Department of Energy under Contract No. DE-AC02-05CH11231.

---

[*] Present address: Diamond Light Source, Didcot OX11 0DE, United Kingdom

[†] Corresponding author: rossnagel@physik.uni-kiel.de

[1] J. A. Wilson, F. J. Di Salvo, and S. Mahajan, Adv. Phys. **24**, 117 (1975).

[2] R. Corcoran, P. Meeson, Y. Onuki, P.-A. Probst, M. Springford, K. Takita, H. Harima, G. Y. Guo, and B. L. Gyorffy, J. Phys.: Condens. Matter **6**, 4479 (1994).

[3] K. Rossnagel, O. Seifarth, L. Kipp, M. Skibowski, D. Voß, P. Krüger, A. Mazur, and J. Pollmann, Phys. Rev. B **64**, 235119 (2001).

[4] M. D. Johannes, I. I. Mazin, and C. A. Howells, Phys. Rev. B **73**, 205102 (2006).

[5] D. E. Moncton, J. D. Axe, and F. J. DiSalvo, Phys. Rev. B **16**, 801 (1977).

[6] C. L. Huang, J.-Y. Lin, Y. T. Chang, C. P. Sun, H. Y. Shen, C. C. Chou, H. Berger, T. K. Lee, and H. D. Yang, Phys. Rev. B **76**, 212504 (2007).

[7] E. Boaknin, M. A. Tanatar, J. Paglione, D. Hawthorn, F. Ronning, R. W. Hill, M. Sutherland, L. Taillefer, J. Sonier, S. M. Hayden, and J. W. Brill, Phys. Rev. Lett. **90**, 117003 (2003).

[8] M. Zehetmayer and H. W. Weber, Phys. Rev. B **82**, 014524 (2010).

[9] J. D. Fletcher, A. Carrington, P. Diener, P. Rodière, J. P. Brison, R. Prozorov, T. Olheiser, and R. W. Giannetta, Phys. Rev. Lett. **98**, 057003 (2007).

[10] C. Wang, B. Giambattista, C. G. Slough, R. V. Coleman, and M. A. Subramanian, Phys. Rev. B **42**, 8890 (1990).

[11] H. F. Hess, R. B. Robinson, and J. V. Waszczak, Physica B **169**, 422 (1991).

[12] I. Guillamon, H. Suderow, F. Guinea, and S. Vieira, Phys. Rev. B **77**, 134505 (2008).

[13] Y. Noat, T. Cren, F. Debontridder, D. Roditchev, W. Sacks, P. Toulemonde, and A. San Miguel, Phys. Rev. B **82**, 014531 (2010).

[14] T. Yokoya, T. Kiss, A. Chainani, S. Shin, M. Nohara, and H. Takagi, Science **294**, 2518 (2001).

[15] T. Valla, A. V. Fedorov, P. D. Johnson, P.-A. Glans, C. McGuinness, K. E. Smith, E. Y. Andrei, and H. Berger, Phys. Rev. Lett. **92**, 086401 (2004).

[16] T. Kiss, T. Yokoya, A. Chainani, S. Shin, T. Hanaguri, M. Nohara, and H. Takagi, Nature Phys. **3**, 720 (2007).

[17] S. V. Borisenko, A. A. Kordyuk, V. B. Zabolotnyy, D. S. Inosov, D. Evtushinsky, B. Büchner, A. N. Yaresko, A. Varykhalov, R. Follath, W. Eberhardt, L. Patthey, and H. Berger, Phys. Rev. Lett. **102**, 166402 (2009).

[18] N. V. Smith, S. D. Kevan, and F. J. DiSalvo, J. Phys. C: Solid State Phys. **18**, 3175 (1985).

[19] K. Rossnagel, E. Rotenberg, H. Koh, N. V. Smith, and L. Kipp, Phys. Rev. B **72**, 121103(R) (2005).

[20] D. S. Inosov, V. B. Zabolotnyy, D. V. Evtushinsky, A. A. Kordyuk, B. Büchner, R. Follath, H. Berger, and S. V. Borisenko, New J. Phys. **10**, 125027 (2008).

[21] D. S. Inosov, D. V. Evtushinsky, V. B. Zabolotnyy, A. A. Kordyuk, B. Büchner, R. Follath, H. Berger, and S. V. Borisenko, Phys. Rev. B. **79**, 125112 (2009).

[22] M. R. Norman, M. Randeria, H. Ding, and J. C. Campuzano, Phys. Rev. B **57**, 11093(R) (1998).

[23] T. Kondo, R. Khasanov, T. Takeuchi, J. Schmalian, and A. Kaminski, Nature (London) **457**, 296 (2009).

[24] E. E. Krasovskii (unpublished).

[25] T. Straub, T. Finteis, R. Claessen, P. Steiner, S. Hüfner, P. Blaha, C. S. Oglesby, and E. Bucher, Phys. Rev. Lett. **82**, 4504 (1999).

[26] W. C. Tonjes, V. A. Greanya, R. Liu, C. G. Olson, and P. Molinié, Phys. Rev. B **63**, 235101 (2001).

[27] D. W. Shen, Y. Zhang, L. X. Yang, J. Wei, H. W. Ou, J. K. Dong, B. P. Xie, C. He, J. F. Zhao, B. Zhou, M. Arita, K. Shimada, H. Namatame, M. Taniguchi, J. Shi, and D. L. Feng, Phys. Rev. Lett. **101**, 226406 (2008).

[28] D. N. Basov and A. V. Chubukov, Nature Phys. **7**, 272 (2011).

[29] B. M. Murphy, H. Requardt, J. Stettner, J. Serrano, M. Krisch, M. Müller, and W. Press, Phys. Rev. Lett. **95**, 256104 (2005).

[30] M. Calandra, I. I. Mazin, and F. Mauri, Phys. Rev. B **80**, 241108(R) (2009).

[31] W. L. McMillan, Phys. Rev. **167**, 331 (1968).

[32] There is also a difference in the variation of the scattering rate Γ_1. This fit parameter is seen to vary between 8 and 12 meV on the Γ-A-centered Fermi contours and between 10 and 30 meV on the K-H pockets.

[33] J. A. Wilson, Phys. Rev. B **15**, 5748 (1977).

[34] M. D. Johannes and I. I. Mazin, Phys. Rev. B **77**, 165135 (2008).

[35] F. Weber, S. Rosenkranz, J.-P. Castellan, R. Osborn, R. Hott, R. Heid, K.-P. Bohnen, T. Egami, A. H. Said, and D. Reznik, Phys. Rev. Lett. **107**, 107403 (2011).

[36] K. Rossnagel, J. Phys.: Condens. Matter **23**, 213001 (2011).